Original Article

J Korean Soc Radiol 2024;85(2):381-393
https://doi.org/10.3348/jksr.2023.0012
eISSN 2951-0805

JOURNAL of THE KOREAN SOCIETY of RADIOLOGY

Pattern Clustering of Symmetric Regional Cerebral Edema on Brain MRI in Patients with Hepatic Encephalopathy

간성뇌증 환자의 뇌 자기공명영상에서 대칭적인 지역 뇌부종 양상의 군집화

Chun Geun Lim, MD[1,2], Hui Joong Lee, MD[1,2]*

[1]Department of Radiology, Kyungpook National University Hospital, Daegu, Korea
[2]Department of Radiology, School of Medicine, Kyungpook National University, Daegu, Korea

Received January 29, 2023
Revised May 16, 2023
Accepted June 11, 2023

***Corresponding author**
Hui Joong Lee, MD
Department of Radiology, Kyungpook National University Hospital, 130 Dongdeok-ro, Jung-gu, Daegu 41944, Korea.

Tel 82-53-420-5397
Fax 82-53-422-2677
E-mail leehuijoong@knu.ac.kr

Purpose Metabolic abnormalities in hepatic encephalopathy (HE) cause brain edema or demyelinating disease, resulting in symmetric regional cerebral edema (SRCE) on MRI. This study aimed to investigate the usefulness of the clustering analysis of SRCE in predicting the development of brain failure.

Materials and Methods MR findings and clinical data of 98 consecutive patients with HE were retrospectively analyzed. The correlation between the 12 regions of SRCE was calculated using the phi (φ) coefficient, and the pattern was classified using hierarchical clustering using the φ^2 distance measure and Ward's method. The classified patterns of SRCE were correlated with clinical parameters such as the model for end-stage liver disease (MELD) score and HE grade.

Results Significant associations were found between 22 pairs of regions of interest, including the red nucleus and corpus callosum ($\phi = 0.81$, $p < 0.001$), crus cerebri and red nucleus ($\phi = 0.72$, $p < 0.001$), and red nucleus and dentate nucleus ($\phi = 0.66$, $p < 0.001$). After hierarchical clustering, 24 cases were classified into Group I, 35 into Group II, and 39 into Group III. Group III had a higher MELD score ($p = 0.04$) and HE grade ($p = 0.002$) than Group I.

Conclusion Our study demonstrates that the SRCE patterns can be useful in predicting hepatic preservation and the occurrence of cerebral failure in HE.

Index terms Hepatic Encephalopathy; Cerebral Edema; Magnetic Resonance Image

INTRODUCTION

Hepatic encephalopathy (HE) is a severe neuropsychiatric complication associated

with both acute and chronic liver failure (1, 2). MRI is regarded as a very useful tool for understanding the pathophysiology of HE better, and advanced techniques have also provided direct evidence for the pathogenesis of severe liver disease and HE (3, 4). The most frequent MR findings of the brain in patients with chronic liver disease (CLD) are basal ganglia high signal intensity on T1-weighted imaging (T1-WI) without mass effect caused by the deposition of paramagnetic manganese (5). As residual liver function gradually declines into compensatory cirrhosis, basal ganglia T1 hyperintensity related to manganese accumulation is observed, and relatively higher T1 hyperintensity correlates with clinical indices such as whole blood manganese, total bilirubin level, and Child-Pugh score, which could indicate the severity of the portal-systemic shunt (6, 7). However, in certain clinical situations, characteristic symmetric regional cerebral edema (SRCE) can be observed on T2-WI, fluid-attenuated inversion recovery (FLAIR) sequences, or even diffusion-weighted imaging (DWI) with neuropsychiatric deterioration (3).

SRCE, represented by high T2 signal intensity in the cerebral white matter observed in some patients with cirrhosis, is quite similar to that observed in metabolic encephalopathy, in which the pathological bases are axonal loss, demyelination, or Wallerian degeneration (3, 8-11). However, although pathological findings of HE have been reported in experimental animals or post-mortem specimens, there has not been a satisfactory explanation for SRCE (12, 13). Moreover, CLD is often accompanied by chronic abnormalities in kidney and blood vessel conditions, and in many cases, is vulnerable to metabolic syndrome and infectious diseases (14, 15). It has been reported that the etiological factors acting in osmotic demyelination syndrome, such as central pontine myelinolysis (CPM) or extra pontine myelinolysis (EPM), overlap with those acting in acquired chronic hepatocerebral degeneration (ACHD) (16, 17). In particular, various medications are sometimes used to treat medical complications, and a narrow therapeutic range of drugs can cause brain lesions, which can lead to confusion in determining the mechanism of brain lesions (18).

SRCE was not always found in HE, and histologically, it was considered mild to moderate myelin and axon loss (13). Metabolic abnormalities in astrocytes due to CLD cause cell edema or demyelinating diseases, resulting in changes in the signal intensity on DWI or T2-WI. To understand the natural clinical history of SRCE in HE, it is important to find associations between brain lesions and meaningfully classify patterns before matching the causes. The present study aimed to investigate the usefulness of predicting the development of brain failure through clustering analysis of SRCE patterns in brain MRI of patients with HE.

MATERIALS AND METHODS

PATIENT POPULATION

The Institutional Review Board of Kyungpook National University Hospital approved this retrospective data collection and analysis (IRB No. KNUH 2022-04-004). The need for informed consent was waived owing to the retrospective design of the study.

From January 2005 to December 2020, we retrospectively reviewed the MRI findings and clinical and MR features of 98 consecutive liver cirrhosis patients (58 male and 40 female; mean age = 58.9 years). HE is defined as a brain dysfunction caused by liver insufficiency

and/or portal-systemic blood shunting. Patients with any other neuropathological evidence except HE, such as tumor, cerebrovascular accident, neurodegenerative disease (for example, Alzheimer's disease or Parkinson's disease), or trauma, were excluded from the study, regardless of the presence of a liver disorder. Patients with congenital metabolic encephalopathy, such as Wilson's disease, were also excluded. Causes of liver disorders were viral hepatitis (n = 51) caused by hepatitis B virus (n = 36) or hepatitis C virus (n = 15), chronic alcoholism (n = 31), autoimmune hepatitis (n = 2), drug-induced hepatitis (n = 3), primary biliary cholangitis (n = 2), and hepatitis of unknown origin (n = 9).

CLINICAL DATA

We obtained laboratory data regarding the onset of symptoms before clinical correction. We reviewed the clinical data from the medical records, including the Glasgow Coma Scale and West-Haven criteria for encephalopathy status (11). We also assessed the laboratory data, including serum bilirubin, aspartate transaminase (AST), alanine transferase, serum creatinine, and international normalized ratio (INR) on admission and then calculated the model for end-stage liver disease (MELD) score to evaluate the hepatic function reserve (19). Cerebral failure was defined as grade III or IV HE according to the West Haven classification (18). Diagnosis of liver failure was based on a serum bilirubin level of $\geq$ 12.0 mg/dL. Kidney failure was defined as a serum creatinine level of $\geq$ 2.0 mg/dL or the need for renal replacement therapy. Coagulation failure was defined as an INR of $\geq$ 2.5 and/or platelet count of $\leq$ 20000/cc.

IMAGE INTERPRETATION

The MR imaging examinations were performed on four different 3T scanners using a standard protocol that included axial T1WI, T2WI, FLAIR, and DWI with apparent diffusion coefficient (ADC) maps. Two neuroradiologists (C.G.L. and H.J.L.), who were blinded to the clinical presentation and outcome, determined the high signal intensities in the twelve regions of interest, including periventricular white matter (PVWM), corpus callosum, internal capsule (known as the representative of the corticospinal tract), corpus striatum, globus pallidus, thalamus, pons, crus cerebri, tegmentum, red nucleus, tectum, and dentate nucleus of the cerebellum, on T2-WI and DWI of the brain by consensus (Fig. 1). Neuroradiologists excluded asymmetric high-signal lesions that were not expected in systemic diseases. For quantitative analysis of the signal intensity of the globus pallidus, two operator-defined region-of-interests (ROIs) were placed in the globus pallidus and the ipsilateral subcortical frontal white matter. The pallidal index was calculated by dividing the mean signal intensity of the globus pallidus by that of the subcortical frontal white matter. Signal intensity measurements of the globus pallidus and frontal white matter on T1-weighted images were conducted by a neuroradiologist (H.J.L.) with 20 years of experience and a neuroradiology fellow (C.G.L.).

STATISTICAL ANALYSIS

Two groups (viral vs. non-viral) were compared in relation to demographic data, laboratory results, and clinical outcomes using the two-sample t-test and Pearson's Chi-square test, as appropriate. Correlations between each ROI were calculated using Phi (ϕ) coefficients. Hierarchical clustering was performed with phi-square (ϕ^2) measure of distance and the Ward

Fig. 1. MR imaging of symmetric regional cerebral edema.
A-D. T2-weighted imaging (left), diffusion-weighted imaging (middle) and apparent diffusion coefficient map (right) at the level of corpus callosum (arrows) (A), striatum (arrows) and periventricular white matter (double arrows) (B), corticospinal tract (arrows) (C), and dentate nucleus (arrows) (D).

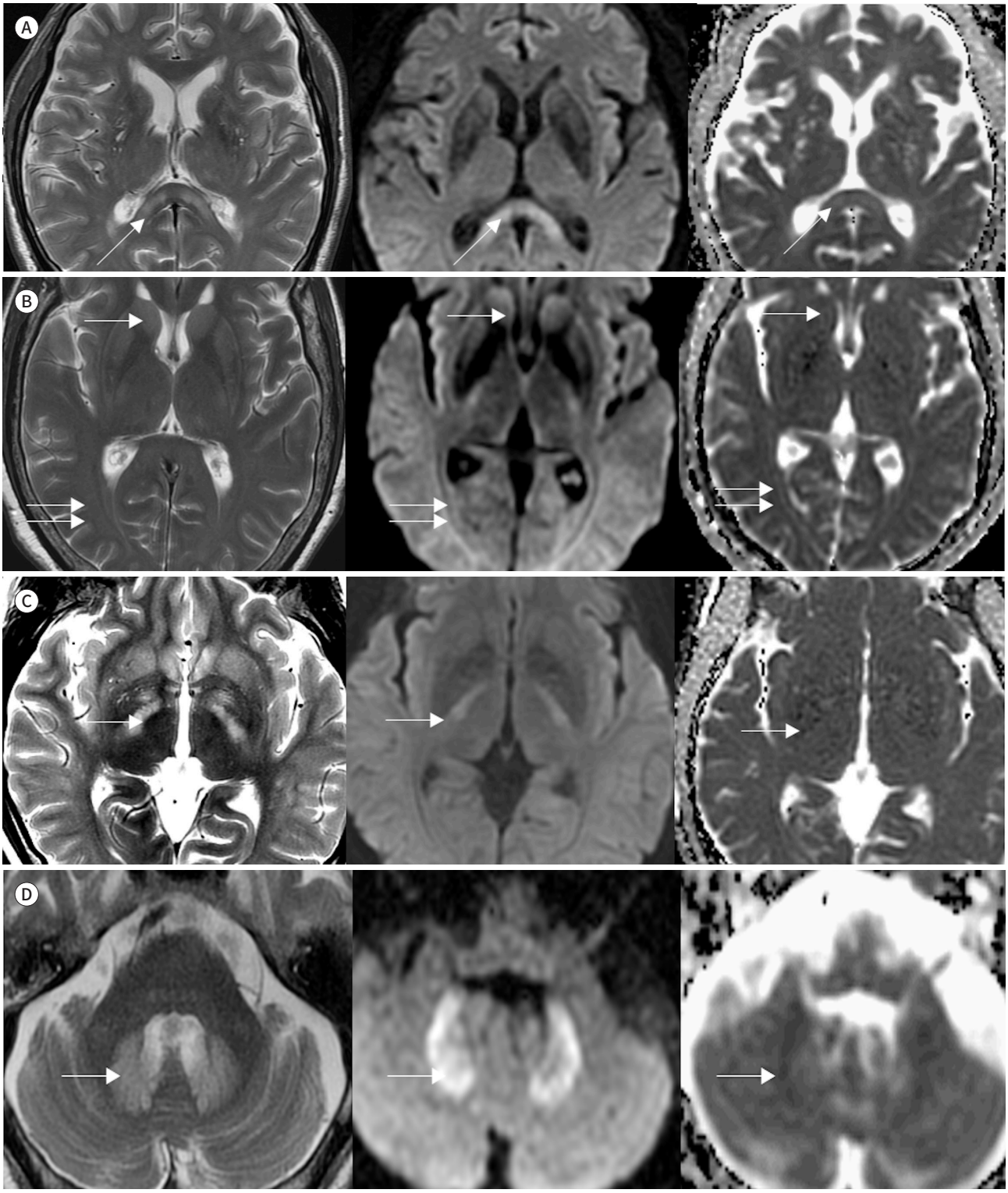

method to classify HE with similar ROI in the study group. The hierarchical cluster analysis results are presented as a dendrogram for variables for brain regions, and the patients were divided into three groups. Clinical data and MRI findings were compared between the identified groups using ANOVA variance and post-hoc Bonferroni correction. All analyses were performed using commercial SPSS software version 20 (IBM Corp., Armonk, NY, USA). Statistical significance was set at $p < 0.004$ to compare the 12 regions. $p \leq 0.05$ for clinical and demographic characteristics was considered statistically significant (Bonferroni post hoc correction, corrected threshold at 0.05/12).

RESULTS

The demographic and clinical characteristics of the patients with overt HE are shown in Table 1. The 53 patients had a chronic viral infection and 45 patients had non-viral causes such as alcoholism. HE with viral infection included 22 male and 31 female with a mean age of 60.40 ± 10.13 years. The 45 patients with nonviral causes included 36 male and 9 female with a mean age of 57.18 ± 11.90 years. The except serum alanine transferase level ($p = 0.006$) and serum ammonia ($p = 0.026$) were higher in the nonviral group. The MELD score ($p = 0.039$) was also higher than in the viral group.

The results obtained by the two evaluators were compared to control for inter-observer error. The inter-rater intraclass correlation coefficient values for signal intensity measurements were 0.996 for the globus pallidus and 0.993 for the white matter of the right frontal lobe, in-

Table 1. Demographic Analysis of Hepatic Encephalopathy

	Viral ($n = 53$)	Non-Viral ($n = 45$)	p-Value
Sex, male:female	22:31	36:9	0.001
Age (years)	60.40 ± 10.13	57.18 ± 11.90	0.142
Na (mmol/L)	131.44 ± 9.19	137.60 ± 6.41	0.054
K (mmol/L)	4.26 ± 0.78	4.00 ± 0.87	0.457
BUN (mg/dL)	19.37 ± 15.18	15.98 ± 10.54	0.132
Creatinine (mg/dL)	1.12 ± 1.38	1.05 ± 0.53	0.125
AST (unit/L)	58.86 ± 33.06	73.41 ± 73.68	0.006
ALT (unit/L)	25.69 ± 18.06	31.93 ± 25.88	0.056
S-ammonia (μmol/L)	56.25 ± 46.80	94.91 ± 93.04	0.026
Glucose (mg/dL)	191.22 ± 155.50	182.69 ± 127.67	0.347
Total bilirubin (mg/dL)	4.25 ± 3.93	3.11 ± 3.08	0.082
Direct bilirubin (mg/dL)	2.22 ± 2.53	1.73 ± 2.57	0.636
Serum albumin (g/dL)	3.20 ± 2.37	3.16 ± 0.52	0.080
Initial GCS	13.66 ± 2.80	14.02 ± 2.02	0.080
Follow up GCS at discharge	12.13 ± 4.78	12.39 ± 4.89	0.823
HE grade	1.32 ± 1.65	1.20 ± 1.57	0.297
MELD score	14.06 ± 7.24	10.79 ± 5.18	0.039

Data are expressed as mean ± standard deviation.
Viral: seropositive of HBs antibody or HCV antigen. Non-viral: include one case of unknown cause. $p < 0.05$: statistically significant.
ALT = alanine transferase, AST = aspartate transaminase, BUN = blood urea nitrogen, GCS = Glasgow coma scale, HE = hepatic encephalopathy, MELD = model for end-stage liver disease, Na = serum sodium

dicating high inter-reliability.

Heatmap and ϕ correlation matrices were calculated for 98 patients among the 12 brain regions on T2-WI and DWI. These ϕ coefficients are comparable to the correlation coefficients and can have values between −1 and 1. Significant associations ($p < 0.004$) on T2-WI were observed particularly between 22 pairs of regions of interest, including the red nucleus and corpus callosum (ϕ = 0.81, $p < 0.001$), the crus cerebri and red nucleus (ϕ = 0.72, $p < 0.001$), and the red nucleus and dentate nucleus (ϕ = 0.66, $p < 0.001$). Significant associations ($p < 0.004$) on DWI were observed between 18 pairs for the crus cerebri and corpus callosum (ϕ = 0.79, $p < 0.001$), red nucleus and corpus callosum (ϕ = 0.69, $p < 0.001$), and red nucleus and dentate nucleus (ϕ = 0.69, $p < 0.001$) (Fig. 2).

Subsequently, based on the affected ROI of the image, the brain image results were classified using hierarchical clustering. This clustering identified distinct groups of radiological features that were uniquely clustered based on the connectivity between the brain lesions (Fig. 3). In Fig. 3, the far upper branch (designated III) segregated the main radiologic features associated with the crus cerebri, red nucleus, corpus callosum, dentate nucleus, and corticospinal tract; the middle branch (designated as I) with the tegmentum and tectum of the midbrain, and the lower (designated as II) with PVWM, pallidus, putamen, thalamus, and pons. Group I showed no signal change in the PVWM and subtle signal changes in a limited ROI, such as the midbrain and pons. Group II showed multiple lesions in the PVWM and the basal ganglia. Group III showed advanced lesions, such as red nucleus and dentate nucleus, in addition to the areas shown in group II (Fig. 4).

After hierarchical clustering, 24 patients were classified into Group I, 35 cases into Group II,

Fig. 2. Heatmaps of Phi correlation among the twelve regions of interest on T2-weighted imaging (A) and diffusion-weighted imaging (B), phi index ranges from -1 to +1: pink indicates a positive correlation (darker pink indicates a stronger correlation); white indicates a no correlation or negative correlation.
Dentate N. = dentate nucleus, PVWM = periventricular white matter, Red N. = red nucleus

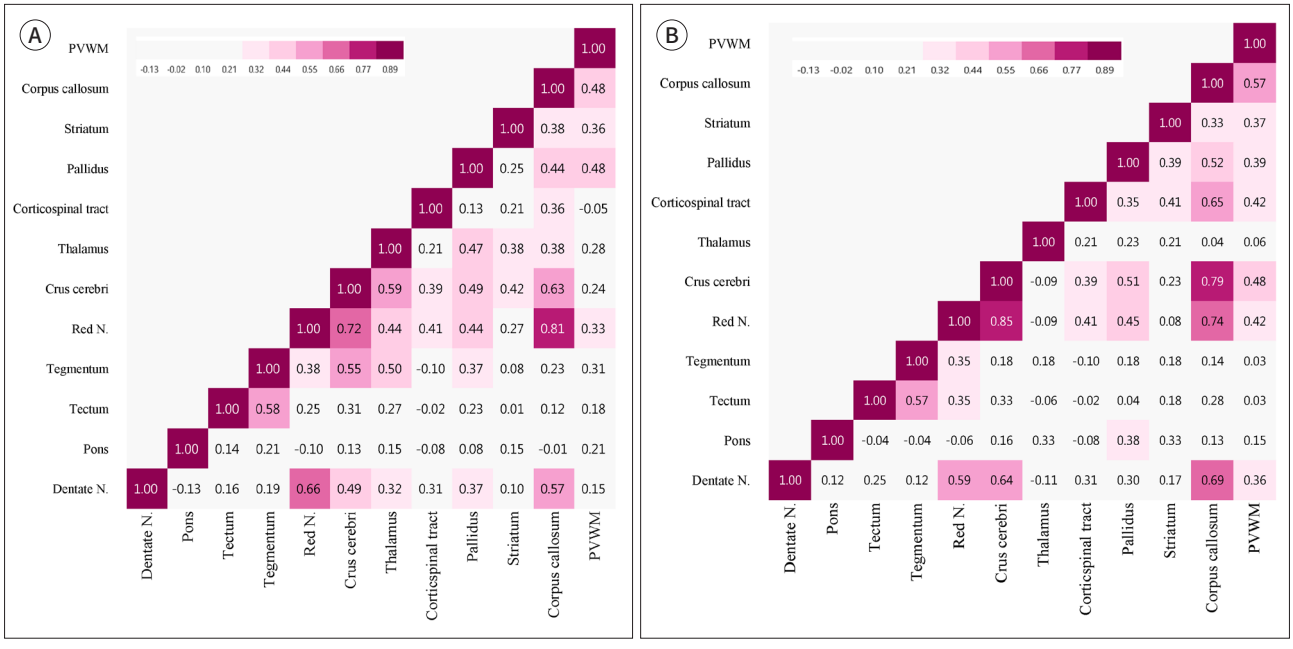

Fig. 3. Clustering of symmetric regional brain edema with hepatic encephalopathy. The dendrogram on the right obtained from the hierarchical clustering of the twelve regions of brain. The color map at the left indicates the number of the involvement region of the brain for each group.
Dentate N. = dentate nucleus, PVWM = periventricular white matter, Red N. = red nucleus

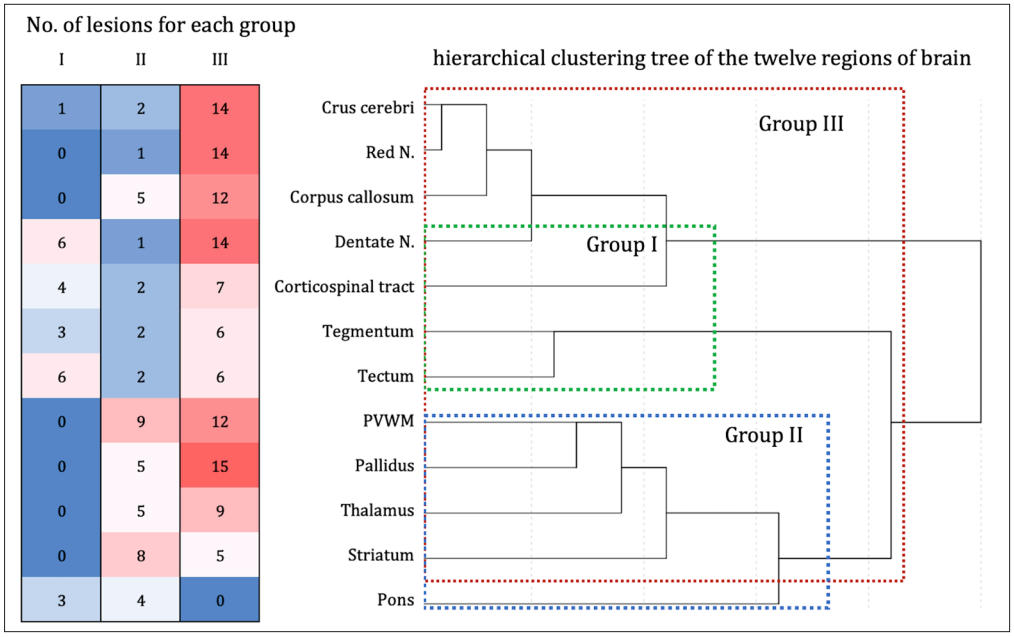

and 39 cases into Group III. ANOVA with post-hoc Bonferroni correction revealed statistically significant differences between the applied groups in AST (Group II and III, $p = 0.043$), platelet count (Group II and III, $p = 0.001$), PI (Group I and III, $p = 0.014$), and MELD score (Group I and III, $p = 0.040$). Cerebral failure developed during the clinical course in 21 of 39 (53.8%) patients (Table 2). The number of affected ROI was higher in Group III than in Group I ($p = 0.014$) and Group II ($p = 0.041$) (Fig. 5).

DISCUSSION

As hepatic function gradually declines into compensatory cirrhosis, intracellular glutamine accumulation and deficiency of choline and myoinositol induce the signal change of gray matter as well as white matter, mimicking the MRI features of amyotrophic lateral sclerosis (8). At the molecular level, two different types of cerebral edema may exist in liver failure: an acute form of cytotoxic edema and a chronic form of vasogenic edema. In liver dysfunction, astrocytes in the brain play a significant role in ammonia detoxification by converting it to glutamine under the catalysis of glutamine synthase, which contributes to increased osmotic pressure (20). However, astrocyte swelling may not occur immediately because of osmotic-regulatory mechanisms that result from the depletion of intracellular osmolytes until decompensation. In acute liver failure, mean diffusivity values are reduced, therefore supporting an increased cell volume secondary to a massive intra-astrocytic increase of glutamine as the mechanism of brain edema. Therefore, the increased cell volume in response to an increase in the mass of glutamine in astrocytes supports the pathogenesis of cytotoxic edema (21). In contrast, in chronically advanced liver failure, altered expression

Fig. 4. T2-weight MR images of each three groups.
A. MR images of patient of Group I shows that affected regions were limited to the midbrain (arrow) and pons (arrowhead) without involvement of periventricular white matter.
B. MR images of patient of Group II reveals multifocal hyperintensities in periventricular white matter (arrow), basal ganglia (arrowhead), thalamus (double arrows), and pons (large arrow).
C. MR images of patient of Group III show extensive involvement in periventricular white matter (arrow), basal ganglia (arrowhead), corpus callosum (large arrowhead), thalamus (short arrow), midbrain (double arrows), also dentate nucleus (large arrow).

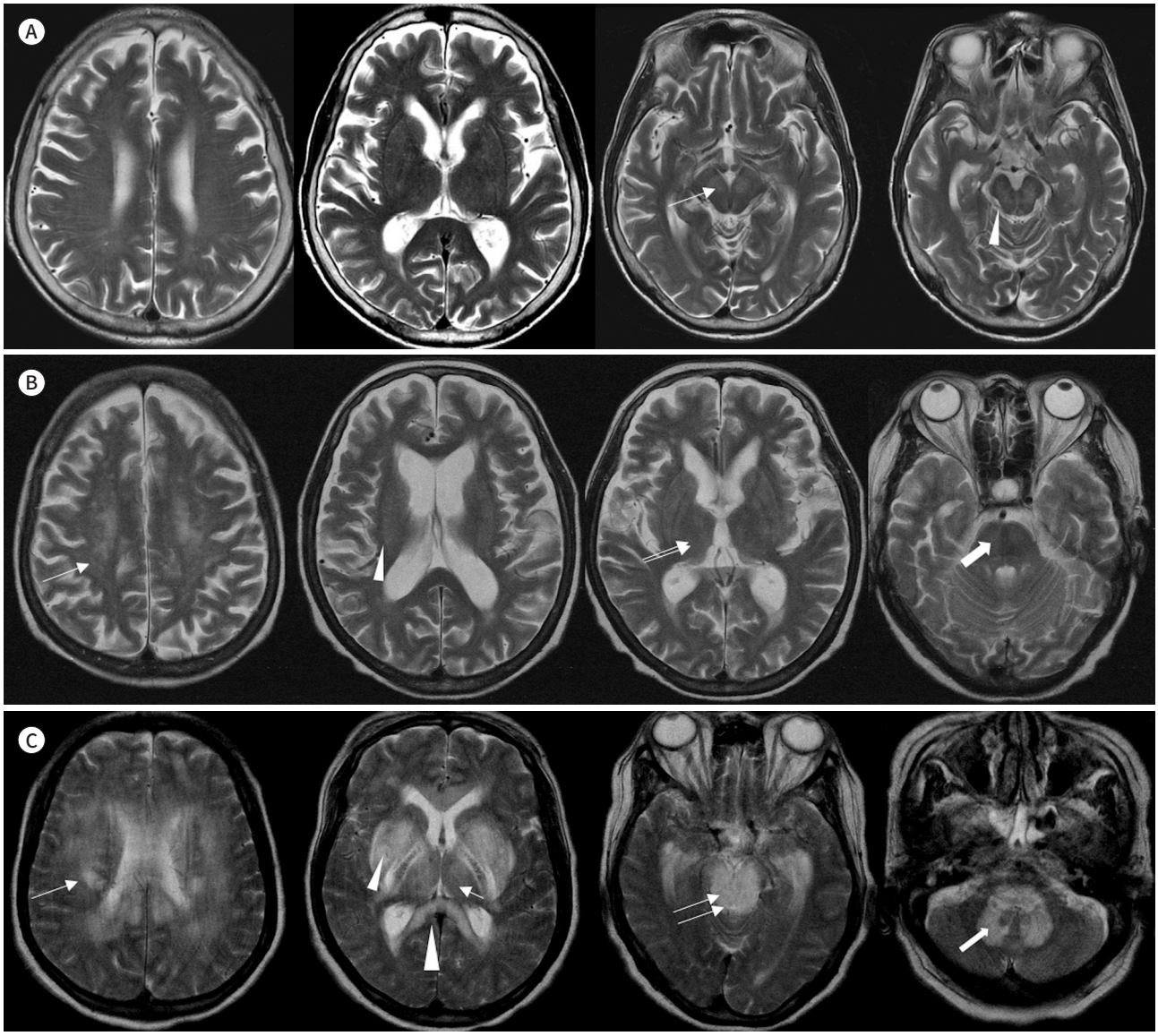

of glutamate transporters in astrocytes may result in decreased intracellular transport of glutamate, resulting in vasogenic edema. Moreover, reduced expression of glial fibrillary acidic proteins induces morphological changes in astrocytes, promoting water diffusivity in the extracellular space. However, it is not easy to understand the causes of various signal changes seen in various areas of MR images of patients with HE and their clinical implications. Owing to different pathological mechanisms and conditions, lesions with high signal intensity along the hemispheric white matter in or around the corticospinal tract on T2-WI may show

Table 2. Characteristics of Patients with Radiological Subgroup

	Group I (*n* = 24)	Group II (*n* = 35)	Group III (*n* = 39)	*p*-Value	Post Hoc < 0.05 (*p*-Value)
Sex, male:female	14:10	23:12	21:18	0.581	
Age (years)	57.17 ± 13.39	60.29 ± 9.80	58.77 ± 10.61	0.568	
Cause of cirrhosis					
Viral:non-viral	12:12	18:17	23:16	0.762	
Laboratory data					
Na (mmol/L)	132.81 ± 9.67	137.03 ± 6.25	132.77 ± 9.24	0.072	
BUN (mg/dL)	18.68 ± 10.27	14.26 ± 5.47	20.46 ± 18.32	0.132	
Creatinine (mg/dL)	0.91 ± 0.73	1.00 ± 0.42	1.26 ± 1.53	0.406	
AST (unit/L)	76.86 ± 59.76	46.74 ± 23.78	76.46 ± 69.84	0.041	II & III (0.043)
ALT (unit/L)	32.30 ± 22.54	25.31 ± 18.79	29.35 ± 24.80	0.487	
PLT (10^3/μL)	95.45 ± 65.94	130.00 ± 86.51	71.27 ± 43.74	0.002	II & III (0.001)
Glucose (mg/dL)	175.50 ± 126.68	191.90 ± 140.10	187.78 ± 149.40	0.943	
S-ammonia (μmol/L)	70.00 ± 50.58	97.48 ± 106.22	62.03 ± 54.91	0.218	
MELD score	10.52 ± 6.04	11.57 ± 4.71	14.68 ± 7.29	0.043	I & III (0.040)
Organ failure					
Cerebral	2	11	18	0.007	
Hepatic	1	3	5	0.570	
Renal	3	3	7	0.490	
Coagulation	0	1	5	0.072	
HE grade	0.46 ± 0.88	1.20 ± 1.61	1.82 ± 1.76	0.004	I & III (0.002)
Pallidal index	1.17 ± 0.09	1.19 ± 0.12	1.21 ± 0.11	0.343	
No. lesion of interest	0.96 ± 1.04	1.40 ± 2.23	2.85 ± 3.55	0.013	I & III (0.014), II & III (0.041)

p < 0.05: statistically significant.
ALT = alanine transferase, AST = aspartate transaminase, BUN = blood urea nitrogen, HE = hepatic encephalopathy, MELD = model for end-stage liver disease, Na = serum sodium, PLT = platelet count

Fig. 5. Comparison of MELD score (A) and HE score (B) according to classified group.
A. Box and whisker plot comparison of MELD score for each group by one-way ANOVA test with Bonferroni post-hoc.
B. Simple error bar graph showed the difference in average of HE grades for each group.
HE = hepatic encephalopathy, MELD = model for end-stage liver disease

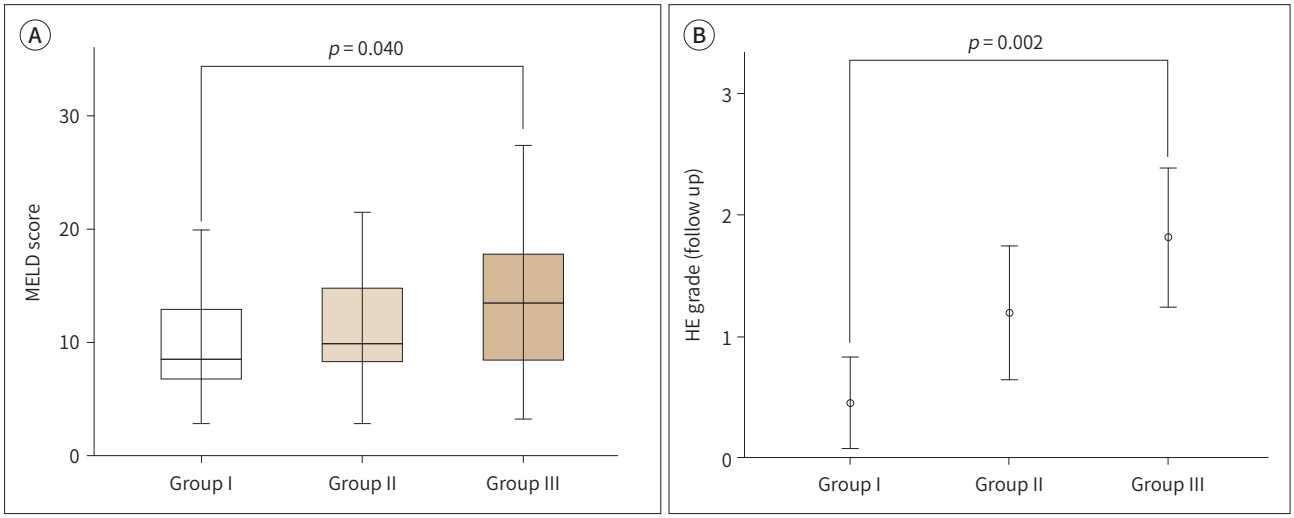

high or normal signal intensity on DWI (3).

According to the concept of acute-chronic liver failure (ACLF), a new disease entity, it is difficult to clearly distinguish the acute phase from the chronic phase of HE (22). In the ACLF conceptual model, the classification of episodes of acute decompensation resulting in organ damage by reducing liver functional depots will help to understand the complexity of cerebral edema. This study hypothesizes is that the grouping of images of SRCE on brain MRI could be related to clinical data of MELD as a marker for the preservation of liver function and HE grade for cerebral failure.

Based on the affected ROI of the image, the brain image results were classified into three patterns using hierarchical clustering. Considering the clinical severity, it was classified into three types: the case with the mildest lesion was defined as Group I, and the case with the most severe form was defined as Group III. In the case of Group I, most of the cases were affected by a small number of areas in various parts of the brain. This group was not included in the main group because only one lesion in the tegmentum or tectum was observed in CLD patients. Since typical Wernicke's encephalopathy was excluded from this study, the possibility that atypical Wernicke's encephalopathy was included cannot be excluded. In addition, patients with CLD are sensitive to damage caused by an osmotic imbalance or external toxic substances; therefore, it may be confused with reversible metabolic disease (23). Patients in this group had a mild clinical course and a relatively good prognosis.

In Group II, lesions were observed in the PVWM, pallidus, striatum, and pons, and the lesions were similar to those in osmotic brain injury. Patients with chronic liver failure are prone to hyponatremia and are very vulnerable to osmolar injuries such as CPM or EPM (17, 24, 25). CPM was first reported as a "hitherto undescribed disease" in 1959 and was characterized by a single, symmetric, midline lesion of the basis pons with myelin breakdown, macrophage influx, relative preservation of nerve cells, and no sign of inflammation in four patients with alcoholism (26). In 1965, the same researchers described "acquired chronic HE" in patients with chronic liver failure (27). It is characterized by the destruction of the myelin sheath in the pontine and extrapontine areas of the brain, including the cortex, subcortex, cerebellum, and thalamus. Considering this historical background, it can be hypothesized that CLD develops into acquired HE (ACHD) in a specific area of the brain that is susceptible to osmotic injury.

Group III, the most severe pattern, was the simultaneous involvement of the corpus callosum-cerebral-red nucleus-dentate nucleus axis, which is mainly connected to the projection fiber. Transcallosal white matter involvement, also known as Marchiafava-Bignami disease (MBD), is a typical form of white matter involvement in patients with hepatic failure (28-30). In this group, there were many affected areas in the lesion, the MELD score was high, and the prognosis was poor. This group shared imaging findings with metabolic encephalopathies, such as MBD or metronidazole encephalopathy (31, 32). In our study, the MELD score and West-Haven criteria, which are indicators of ACLF, were significantly higher in Group III, suggesting an association between SRCE and ACLF. After entering decompensated cirrhosis, white matter T2 hypersensitivity is observed on MRI (17, 33). The most severe form of ACLF progresses rapidly to intracranial hypertension and cerebral edema, leading to coma or death; however, MR findings of cerebral edema related to ACLF have not been established (34).

This study had several limitations. First, this study included patients who underwent MRI at a single tertiary referral hospital. However, we were unable to obtain sufficient brain MR images of patients with CLD but without HE since brain MR is not mandatory in these patients. The most common underlying disease included in this study was HBV-related hepatitis. The underlying precipitating factors differ around the world, with viral hepatitis being predominant in Asia and drug-induced liver damage being predominant in North America and Europe. Second, we did not perform quantitative evaluation, such as ADC value, and we did not consider that there may be a difference in the severity of edema even though it is the same regional lesion. Third, our results could not be verified by pathological correlations owing to disease specificity. Therefore, a prospective study is recommended to clarify our hypothesis for this disease population, as the diagnosis itself should be based on radiological patterns and a general consensus based on a clinical review should be adopted. This could be a concern for selection bias in study interpretation.

Despite these limitations, this study presented a methodology for classifying the imaging findings of HE, and it can be summarized that it helped establish a classification system for HE by showing a correlation with the clinical course. As a result of the present study, the SRCE was classified into three patterns using hierarchical clustering analysis. One showed minimal involvement of the brainstem, another showed involvement of the basal ganglia and pons, and another pattern affected structures, including the red nucleus dentate nucleus connected to projection fibers, resulting in a poor prognosis. Our study demonstrated that clustering analysis of SRCE patterns on MRI can be useful in predicting the occurrence of cerebral failure in patients with HE. These findings suggest that this approach could be a valuable tool for hepatic preservation and monitoring the progression of HE.

Availability of Data and Material

The datasets generated or analyzed during the study are available from the corresponding author on reasonable request.

Author Contributions

Conceptualization, all authors; data curation, L.H.J.; formal analysis, all authors; investigation, L.H.J.; methodology, all authors; project administration, L.H.J.; resources, L.H.J.; software, all authors; supervision, L.H.J.; validation, L.H.J.; visualization, L.H.J.; writing—original draft, all authors; and writing—review & editing, all authors.

Conflicts of Interest

The authors have no potential conflicts of interest to disclose.

ORCID iDs

Chun Geun Lim https://orcid.org/0000-0002-5876-659X
Hui Joong Lee https://orcid.org/0000-0002-1279-3795

Funding

None

REFERENCES

1. Hazell AS, Butterworth RF. Hepatic encephalopathy: an update of pathophysiologic mechanisms. *Proc*

Soc Exp Biol Med 1999;222:99-112
2. Sherlock S. Hepatic encephalopathy. *Br J Hosp Med* 1977;17:144-146, 151-154, 159
3. Rovira A, Alonso J, Córdoba J. MR imaging findings in hepatic encephalopathy. *AJNR Am J Neuroradiol* 2008;29:1612-1621
4. Kreis R, Farrow N, Ross BD. Localized 1H NMR spectroscopy in patients with chronic hepatic encephalopathy. Analysis of changes in cerebral glutamine, choline and inositols. *NMR Biomed* 1991;4:109-116
5. Inoue E, Hori S, Narumi Y, Fujita M, Kuriyama K, Kadota T, et al. Portal-systemic encephalopathy: presence of basal ganglia lesions with high signal intensity on MR images. *Radiology* 1991;179:551-555
6. Lee DH, Lee HJ, Hahm MH. The pallidal index in patients with acute-on-chronic liver disease: is it a predictor of severe hepatic encephalopathy? *Investig Magn Reson Imaging* 2017;21:125-130
7. Krieger D, Krieger S, Jansen O, Gass P, Theilmann L, Lichtnecker H. Manganese and chronic hepatic encephalopathy. *Lancet* 1995;346:270-274
8. Rovira A, Córdoba J, Sanpedro F, Grivé E, Rovira-Gols A, Alonso J. Normalization of T2 signal abnormalities in hemispheric white matter with liver transplant. *Neurology* 2002;59:335-341
9. Córdoba J, Raguer N, Flavià M, Vargas V, Jacas C, Alonso J, et al. T2 hyperintensity along the cortico-spinal tract in cirrhosis relates to functional abnormalities. *Hepatology* 2003;38:1026-1033
10. Finlayson MH, Superville B. Distribution of cerebral lesions in acquired hepatocerebral degeneration. *Brain* 1981;104(Pt 1):79-95
11. de Oliveira AM, Paulino MV, Vieira APF, McKinney AM, da Rocha AJ, Dos Santos GT, et al. Imaging patterns of toxic and metabolic brain disorders. *Radiographics* 2019;39:1672-1695
12. Soffer D, Sherman Y, Tur-Kaspa R, Eid A. Acquired hepatocerebral degeneration in a liver transplant recipient. *Acta Neuropathol* 1995;90:107-111
13. Matsusue E, Kinoshita T, Ohama E, Ogawa T. Cerebral cortical and white matter lesions in chronic hepatic encephalopathy: MR-pathologic correlations. *AJNR Am J Neuroradiol* 2005;26:347-351
14. vom Dahl S, Kircheis G, Häussinger D. Hepatic encephalopathy as a complication of liver disease. *World J Gastroenterol* 2001;7:152-156
15. Abou-Assi S, Vlahcevic ZR. Hepatic encephalopathy. Metabolic consequence of cirrhosis often is reversible. *Postgrad Med* 2001;109:52-70
16. Kleinschmidt-DeMasters BK, Filley CM, Rojiani AM. Overlapping features of extrapontine myelinolysis and acquired chronic (non-Wilsonian) hepatocerebral degeneration. *Acta Neuropathol* 2006;112:605-616
17. Lim CG, Hahm MH, Lee HJ. Hepatic encephalopathy on magnetic resonance imaging and its uncertain differential diagnoses: a narrative review. *J Yeungnam Med Sci* 2023;40:136-145
18. Blei AT, Córdoba J; Practice Parameters Committee of the American College of Gastroenterology. Hepatic encephalopathy. *Am J Gastroenterol* 2001;96:1968-1976
19. Delis SG, Bakoyiannis A, Biliatis I, Athanassiou K, Tassopoulos N, Dervenis C. Model for end-stage liver disease (MELD) score, as a prognostic factor for post-operative morbidity and mortality in cirrhotic patients, undergoing hepatectomy for hepatocellular carcinoma. *HPB (Oxford)* 2009;11:351-357
20. Albrecht J, Dolińska M. Glutamine as a pathogenic factor in hepatic encephalopathy. *J Neurosci Res* 2001; 65:1-5
21. Desjardins P, Bélanger M, Butterworth RF. Alterations in expression of genes coding for key astrocytic proteins in acute liver failure. *J Neurosci Res* 2001;66:967-971
22. Wright G, Sharifi Y, Jover-Cobos M, Jalan R. The brain in acute on chronic liver failure. *Metab Brain Dis* 2014; 29:965-973
23. Kim HK, Lee HJ, Lee W, Kim YS, Jang HW, Byun KH. Pattern approach to MR imaging in patients with end-stage hepatic failure: a proposal for a new disease entity "hepatic encephalopathy continuum." *Neuroradiology* 2008;50:683-691
24. Praharaj DL, Anand AC. Clinical implications, evaluation, and management of hyponatremia in cirrhosis. *J Clin Exp Hepatol* 2022;12:575-594
25. Schrier RW, Gurevich AK, Cadnapaphornchai MA. Pathogenesis and management of sodium and water retention in cardiac failure and cirrhosis. *Semin Nephrol* 2001;21:157-172
26. Adams R, Victor M, Mancall E. Central pontine myelinolysis: a hitherto undescribed disease occurring in alcoholic and malnourished patients. *AMA Arch Neurol Psychiatry* 1959;81:154-172
27. Victor M, Adams RD, Cole M. The acquired (non-Wilsonian) type of chronic hepatocerebral degeneration.

Medicine (Baltimore) 1965;44:345-396
28. Gabriel S, Grossmann A, Höppner J, Benecke R, Rolfs A. [Marchiafava-Bignami syndrome. Extrapontine myelinolysis in chronic alcoholism]. *Nervenarzt* 1999;70:349-356. German
29. Heinrich A, Runge U, Khaw AV. Clinicoradiologic subtypes of Marchiafava-Bignami disease. *J Neurol* 2004;251:1050-1059
30. Ménégon P, Sibon I, Pachai C, Orgogozo JM, Dousset V. Marchiafava-Bignami disease: diffusion-weighted MRI in corpus callosum and cortical lesions. *Neurology* 2005;65:475-477
31. Hwang E, Chang SK, Lee SA, Choi JA. A case of metronidazole-induced encephalopathy: atypical involvement of the brain on MRI. *Investig Magn Reson Imaging* 2018;22:200-203
32. Kim HJ, Sunwoo MK, Lee JH, Choi YS, Kim DY. Methanol-induced encephalopathy: a case report. *Investig Magn Reson Imaging* 2017;21:61-64
33. Romero-Gómez M, Montagnese S, Jalan R. Hepatic encephalopathy in patients with acute decompensation of cirrhosis and acute-on-chronic liver failure. *J Hepatol* 2015;62:437-447
34. Joshi D, O'Grady J, Patel A, Shawcross D, Connor S, Deasy N, et al. Cerebral oedema is rare in acute-on-chronic liver failure patients presenting with high-grade hepatic encephalopathy. *Liver Int* 2014;34:362-366

간성뇌증 환자의 뇌 자기공명영상에서 대칭적인 지역 뇌부종 양상의 군집화

임춘근[1,2] · 이희중[1,2]*

목적 간성뇌증(hepatic encephalopathy; 이하 HE)의 대사이상은 뇌부종 또는 탈수초성 질환을 일으켜 자기공명영상에서 대칭적인 지역 뇌부종을 유발한다. 본 연구에서 HE 환자의 뇌 자기공명영상에서 대칭적인 지역 뇌부종 패턴의 군집화 분석을 통해 뇌부전 발생 예측의 유용성을 조사하는 것을 목적으로 한다.

대상과 방법 연속적인 HE 환자 98명을 대상으로 MR 소견과 임상자료를 후향적으로 분석하였다. Symmetric regional cerebral edema (이하 SRCE)의 12개 영역 간의 상관관계는 파이(ϕ) 계수를 사용하여 계산하였고, ϕ^2 거리 측정과 Ward의 방법을 사용하여 계층적 군집화를 사용하여 패턴을 분류하였다. SRCE의 분류된 패턴은 말기 간 질환 모델(model for end-stage liver disease; 이하 MELD) 점수 및 HE 등급과 같은 임상과 상관관계를 조사하였다.

결과 적색 핵과 뇌량($\phi = 0.81$, $p < 0.001$), 대뇌 십자 및 적색 핵($\phi = 0.72$, $p < 0.001$), 적색핵과 치상핵($\phi = 0.66$, $p < 0.001$)을 포함한 22쌍의 관심영역 사이에 유의한 연관성이 발견되었다. 계층적 군집화 후 24건을 I군, 35건을 II군, 39건을 III군으로 분류하였다. 그룹 III은 그룹 I에 비해 MELD 점수($p = 0.04$)와 HE 등급($p = 0.002$)이 더 높았다.

결론 본 연구는 HE 환자에서 대칭적인 지역 뇌부종의 패턴은 간 보존 및 뇌부전 발생을 예측하는 데 유용할 수 있음을 보여주었다.

[1]경북대학교병원 영상의학과,
[2]경북대학교 의과대학 영상의학교실